NASA TECHNICAL NOTE

NASA TN D-3410
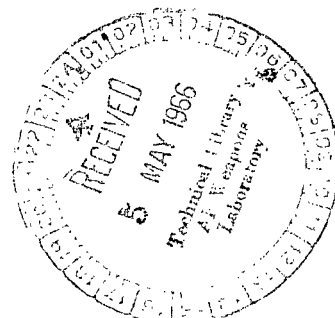
ONE-DIMENSIONAL NONLINEAR MODEL FOR DETERMINING COMBUSTION INSTABILITY IN SOLID PROPELLANT ROCKET MOTORS

by Louis A. Povinelli

Lewis Research Center

Cleveland, Ohio

NATIONAL AERONAUTICS AND SPACE ADMINISTRATION • WASHINGTON, D. C. • APRIL 1966

ONE-DIMENSIONAL NONLINEAR MODEL FOR DETERMINING COMBUSTION

INSTABILITY IN SOLID PROPELLANT ROCKET MOTORS

By Louis A. Povinelli

Lewis Research Center
Cleveland, Ohio

NATIONAL AERONAUTICS AND SPACE ADMINISTRATION

ONE-DIMENSIONAL NONLINEAR MODEL FOR DETERMINING COMBUSTION
INSTABILITY IN SOLID PROPELLANT ROCKET MOTORS

by Louis A. Povinelli

Lewis Research Center

SUMMARY

A nonlinear analysis of combustion instability in a solid propellant rocket geometry was performed by using the Priem-Guentert one-dimensional model composed of a thin annulus. Nondimensionalization of the basic conservation equations yielded three parametric groupings, which were representative of a burning rate, a wall loss, and a viscous loss. The propellant was assumed to react in accordance with the normal steady-state expression and included an erosive burning term. The results of the analysis yielded the minimum pressure amplitude required for instability as a function of the parametric groupings. Erosive burning, a high pressure exponent, and a low axial velocity were found to decrease the stable operating range for rocket motors. The stability boundaries were affected more by erosive burning and axial velocity than by the pressure exponent. The regions of stable motor operation were found to be insensitive to the wall-loss and viscous dissipation parameters.

INTRODUCTION

The subject of solid propellant combustion instability has received a substantial amount of attention both experimentally and theoretically in recent years. Numerous reviews have appeared in the literature. The most recent ones were Trubridge (ref. 1), Hart and McClure (ref. 2), and Price (ref. 3). A status report (1964) by Berl, Hart, and McClure (ref. 4) is also available. These references together summarize the field of solid propellant instability from practical hardware problems to the most recent and sophisticated analysis. These papers (along with those referenced therein) serve to point out the lack of understanding in certain aspects of the field as well as the complexity of the unstable phenomenon occurring in solid propellant rocket motors. A certain degree of experimental success has been achieved in understanding the interaction between the

flow field and the combustion processes (ref. 5). Similarly, linear stability analysis (ref. 6), which considers the participation of the solid phase during instability, has been successful in predicting the intermittent behavior observed during rocket motor firings. Certain quantitative aspects of linear stability theory have been compared with experimental measurements, and limited success has been demonstrated, namely for high pressure combustion of double-base propellants (refs. 7 and 8). Consideration of additional factors in the linear theory, such as the effect of thermal radiation on the propellant response (ref. 9), has improved the agreement between analysis and experiment.

The current understanding of combustion stability, although helpful, is such that a prediction of the unsteady burning behavior of rocket motors is not possible. Consideration of the nonlinearity of the phenomenon may serve to improve our understanding of combustion instability. Recently, nonlinear effects arising from erosive burning have been analyzed. The analysis showed that significant wave form distortions may occur even for relatively small amplitudes of the pressure oscillation (ref. 10). The status of finite amplitude theory is presented in reference 2. The purpose of the present report is to give the results of a nonlinear analysis of the problem of acoustic stability in solid propellant rocket motors by using a one-dimensional model that incorporates the nonlinearities arising from the dependence of burning rate on velocity and pressure, and requirement of finite amplitude pressure disturbances, and the nonlinear terms arising in the conservation equations such as the viscous dissipation effects in the gas. Although the one-dimensional model used does not include all the features of a real rocket motor, its behavior will be helpful in understanding combustion instability in a complete engine. The analysis is limited to the gas modes only and hence is applicable either for the case where the gas cavity is large relative to the propellant thickness (ref. 11) or where the viscous damping in the solid is quite large so that the solid will not sustain resonant motion (refs. 12 and 13). An additional calculation of the combustion stability limit is presented that considers the energy gain or loss due to wall motion.
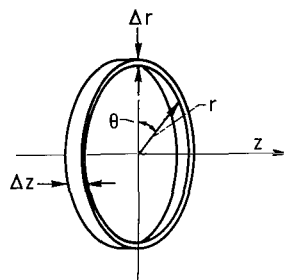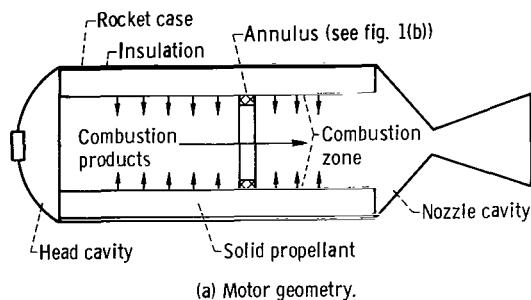
THEORETICAL MODEL

Description of Model

A simple rocket geometry is shown in figure 1(a). It consists of a hollow cylindrical

(a) Motor geometry.

(b) Annular element.

Figure 1. - Geometry of analytical model.

grain extending from the motor-head end to the nozzle entrance with combustion occurring on the inside surface of the grain. The propellant is assumed to be rigidly bound to the outer case which is inflexible. The model used is a thin annulus inside the combustor at the propellant surface (fig. 1(b)), having a thickness Δr and a length Δz. Flow through the annular volume is composed of combustion gases generated both upstream of the annulus and at the solid-gas interface of the annulus. The axial velocity is assumed constant over the cross section of the rocket gas core, and acceleration of the axial flow occurs through the annulus. Gas addition due to combustion is assumed to be added uniformly throughout the combustor volume. A simple power law is assumed that relates the combustion rate to the instantaneous local pressure and gas velocity.

Conservation Equations

The conservation equations are written in terms of the instantaneous value of the flow properties. Perturbation of the flow in the θ-direction is subsequently introduced. The analysis follows the technique of Priem and Guentert (ref. 14) in presenting, for the θ-direction, the pertinent one-dimensional conservation equations with mass addition:

Continuity equation:

$$\frac{\partial \rho}{\partial t} = -\nabla \cdot \rho \vec{v} + \omega \tag{1}$$

Momentum equation:

$$\rho \frac{\partial \vec{v}}{\partial t} = -\rho(\vec{v} \cdot \nabla)\vec{v} - \vec{v}\omega - g\nabla P - \nabla \cdot \tau \tag{2}$$

Energy equation:

$$\rho c_v \frac{\partial T}{\partial t} = -\rho c_v (\vec{v} \cdot \nabla)T + \lambda \nabla^2 T - \frac{P}{J} \nabla \cdot \vec{v} - \frac{1}{gJ} \tau : \nabla \vec{v} + \omega \left(U_s - c_v T + \frac{1}{2gJ} \vec{v} \cdot \vec{v} \right) \tag{3}$$

where the liquid velocity vector that appeared in reference 14 has been omitted. (Symbols are defined in appendix A.) Before proceeding to the nondimensionalization of the conservation equations, the possible contributions due to wall losses will be discussed. As

3

mentioned in the INTRODUCTION, the solid modes of the viscoelectric material as well as the thermal expansion and compressibility of the propellant were not generally considered. This limits the general analysis, therefore, to a consideration of the normal gas modes in the rocket cavity. The applicability of the results presented herein is restricted thereby to either of two situations: namely, (1) where the propellant grain thickness is small relative to the gas cavity radius, or (2) where the viscous damping in the solid is quite large so that the solid will not sustain resonant motion. For the first case the behavior of the gas-solid system corresponds rather closely to a system composed only of gas (ref. 11). For the second case where the viscous damping in the solid is large the impedance mismatch at the solid-gas interface will be large, and practically all the acoustic energy incident on the solid surface will be reflected back into the gas (ref. 12). This energy loss is limited to the amount of energy transmitted into the solid and may be represented by an admittance whose real part is $(\rho_s a_s)^{-1}$ (ref. 13), which is a negligibly small quantity.

In the more complicated situation where the viscoeleastic material participates in the oscillation, the energy loss (or gain) can be calculated by using the results of references 15 and 16 (see appendix B). This loss term may then be subtracted from the right side of the energy equation (3). The effect of this loss term was shown to be negligible.

The transport equations (1), (2), and (3) are now nondimensionalized by means of the following transformations (ref. 14):

$$
\left.
\begin{aligned}
t' &= \frac{ta}{r} & P' &= \frac{P}{P_o} \\[2ex]
\nabla' &= r\nabla & \tau' &= \frac{\tau r}{\mu_o a} \\[2ex]
\omega' &= \frac{\omega}{\omega_o} & T' &= \frac{T}{T_o} \\[2ex]
\rho' &= \frac{\rho}{\rho_o} & v' &= \frac{v}{a}
\end{aligned}
\right\}
\tag{4}
$$

The following nondimensionalized equations result:

Continuity:

$$
\frac{\partial \rho'}{\partial t'} = -\nabla' \cdot \rho' \vec{v}' + \left| \frac{r\omega_o}{\rho_o a} \right| \omega'
\tag{5}
$$

4

Motion:

$$\rho' \frac{\partial \vec{v}'}{\partial t'} = -\rho'(\vec{v}' \cdot \nabla')\vec{v}' - \left|\frac{gP_o}{\rho_o a^2}\right| \nabla' P' - \left|\frac{\mu}{r\rho_o a}\right| \nabla' \cdot \tau' - \left|\frac{r\omega_o}{\rho_o a}\right| (\vec{v}')\omega' \tag{6}$$

Energy:

$$\rho' \frac{\partial T'}{\partial t'} = -\rho'(v' \cdot \nabla')T' + \left|\frac{\lambda}{r\rho_o c_v a}\right| \nabla'^2 T' - \left|\frac{P_o}{\rho_o c_v T_o J}\right| P' \nabla' \cdot \vec{v}'$$

$$- \left|\frac{a\mu}{r\rho_o c_v T_o gJ}\right| \tau' : \nabla' \vec{v}' + \left|\frac{\omega_o r}{\rho_o a}\right| \omega' \left[\frac{U_s}{c_v T_o} - T' + \frac{a^2}{2gJc_v T_o}(\vec{v}')^2\right] - \frac{P_o^2 (P' - 1)^2 r Z_1}{\rho_o c_v T_o a} \tag{7}$$

where

$$P_o(P' - 1) = \frac{A_p}{2} \tag{8}$$

and

$$Z_1 = \pi J_m^2(k_g r_1) \times (\text{Real part admittance}) \tag{9}$$

The admittance may be calculated from the expression given in appendix B or obtained from the results of references 6, 11, 15, and 16. Using the following relations (ref. 14)

$$\left. \begin{array}{ll} gT_o \dfrac{R}{M} \gamma = a^2 & P = \rho \dfrac{R}{M} T \\[2ex] \dfrac{c_v \mu}{\lambda} \cong 1 & U_s = c_v T_o \cong c_p T_o \\[2ex] \dfrac{c_p}{c_v} = \gamma & c_v = \dfrac{R}{JM} \dfrac{1}{\gamma - 1} \end{array} \right\} \tag{10}$$

reduces the grouping of the variables in the conservation equations (6) and (7) to

$$\frac{gP_O}{\rho_O a^2} = \frac{1}{\gamma} \qquad \frac{\lambda}{r\rho_O c_v a} \cong \frac{\mu}{r\rho_O a}$$

$$\frac{P_O}{\rho_O c_v T_O J} = \gamma - 1 \qquad \frac{a\mu}{r\rho_O c_v T_O gJ} = \frac{\mu}{r\rho_O a}\,\gamma(\gamma - 1)$$

$$\tag{11}$$

The dimensionless groups appearing in the preceding conservation equations may be transformed to the usual rocket combustor variables by applying the following expressions (ref. 14):

$$c^* = \frac{P_O A_t g}{w} = \frac{1}{\gamma}\sqrt{\frac{g\gamma R T_O}{M\left(\dfrac{2}{\gamma + 1}\right)^{\gamma+1/\gamma-1}}}$$

$$\omega_O = \frac{w}{V}$$

$$P_O = \rho_O \frac{R}{M} T_O$$

$$a^2 = g\frac{R}{M}\gamma T_O$$

$$w = \rho_s r_s A_s$$

$$r_1 \cong r$$

$$\tag{12}$$

These transformations result in

$$\frac{r\omega_O}{\rho_O a} = \frac{r}{\rho_O a}\frac{2\rho_s r_s}{r} = \frac{2\rho_s r_s}{\rho_O a} \tag{13}$$

and

$$\frac{\mu}{\rho_o ra} = \frac{\mu c^*}{rP_o g} \sqrt{\left(\frac{2}{\gamma + 1}\right)^{\gamma+1/\gamma-1}} \tag{14}$$

The dimensionless groups are now defined as

(1)
$$\frac{2\rho_s r_s}{\rho_o a} = \mathcal{M} \tag{15}$$

When the ideal gas relation, the c^* expression, and the speed of sound relation are substituted into equation (14), this ratio becomes

$$\frac{2A_t}{A_s} \sqrt{\left(\frac{2}{\gamma + 1}\right)^{\gamma+1/\gamma-1}} = \mathcal{M} \tag{16}$$

where A_t/A_s represents the reciprocal of the usual K ratio for solid propellant rocket motors.

(2)
$$\frac{\mu c^*}{rP_o g} = \mathcal{J} \tag{17}$$

(3)
$$\frac{P_o^2 rZ_1}{\rho_o c_v T_o a} = \mathcal{X} \tag{18}$$

The first term $\mathcal{M}$ represents either the burning rate or the K ratio parameter (eq. 16), $\mathcal{J}$ is the viscous dissipation parameter, and $\mathcal{X}$ is the wall-loss parameter.

The transport equations are now written by assuming that the radial velocity and all derivatives in the radial direction are zero, that the axial velocity does not vary with angular position or time, and that $\partial v_\theta' / \partial_z'$ and all second derivatives in the axial direction are zero. For the annular combustor the reduced radial distance r' is always unity. The transport equations are as follows:

Continuity:

$$\frac{\partial \rho'}{\partial t'} = -\rho'\left(\frac{\partial v'_\theta}{\partial \theta'} + \frac{\partial v'_z}{\partial z'}\right) - v'_\theta \frac{\partial \rho'}{\partial \theta'} - v'_z \frac{\partial \rho'}{\partial z'} + \omega'\mathcal{M} \tag{19}$$

Momentum in θ-direction:

$$\rho'\frac{\partial v'_\theta}{\partial t'} = -\rho v'_\theta \frac{\partial v'_\theta}{\partial \theta'} - \left|\frac{1}{\gamma}\right|\frac{\partial P'}{\partial \theta'} + \mathcal{J}f(\gamma)\frac{4}{3}\frac{\partial^2 v'_\theta}{(\partial \theta')^2} - v'_\theta \omega'\mathcal{M} \tag{20}$$

Momentum in z-direction:

$$0 = -\rho' v'_z \frac{\partial v'_z}{\partial z'} - \left|\frac{1}{\gamma}\right|\frac{\partial P'}{\partial z'} - \mathcal{M}v'_z \omega' \tag{21}$$

Energy:

$$\rho'\frac{\partial T'}{\partial t'} = -\rho'\left(v'_\theta \frac{\partial T'}{\partial \theta'} + v'_z \frac{\partial T'}{\partial z'}\right) + \mathcal{J}f(\gamma)\frac{\partial^2 T'}{(\partial \theta')^2} - |\gamma - 1|\ P'\left(\frac{\partial v'_\theta}{\partial \theta'} + \frac{\partial v'_z}{\partial z'}\right)$$

$$+ \frac{4}{3}|\gamma(\gamma - 1)|\ \mathcal{J}\left[\left(\frac{\partial v'_\theta}{\partial \theta'}\right)^2 + \left(\frac{\partial v'_z}{\partial z'}\right)^2 - \frac{\partial v'_\theta}{\partial \theta'}\frac{\partial v'_z}{\partial z'}\right]f(\gamma)$$

$$+ \mathcal{M}\omega'\left\{\gamma - T' + \frac{(\gamma - 1)\gamma}{2}\left[v'^2_z + v'^2_\theta\right]\right\} - (P' - 1)^2 \tag{22}$$

Ideal gas:

$$\frac{\partial P'}{\partial \theta'} = T'\frac{\partial \rho'}{\partial \theta'} + \rho'\frac{\partial T'}{\partial \theta'} \tag{23}$$

where $\theta' = \theta$ and $z = z'$.

In order to evaluate the derivatives in the axial direction, the conservation equations are integrated through the entire volume of the annulus. None of the terms in the axial or radial direction were assumed to vary. In addition, the total mass, momentum, and

8

energy in the annulus are invariant with time, and none of the terms vary in the small distances $\Delta r'$ and $\Delta z'$. The only derivatives allowed in the z'-direction are $\partial T'/\partial z'$, $\partial v_z'/\partial z'$, $\partial \rho'/\partial z'$, and $\partial P'/\partial z'$, and they do not vary with angular position. There is no net loss nor gain of mass, momentum, and energy fluxes in the angular direction since the annulus is closed (ref. 14). The following expressions, therefore, permit the evaluation of the derivatives with respect to z':

Continuity:

$$\frac{\partial v_z'}{\partial z} \int_0^{2\pi} \rho' \, d\theta' + 2\pi v_z' \frac{\partial \rho'}{\partial z'} = \mathscr{M} \int_0^{2\pi} \omega' \, d\theta' \tag{24}$$

Momentum:

$$v_z' \frac{\partial v'}{\partial z'} \int_0^{2\pi} \rho' \, d\theta' + \frac{1}{\gamma}\left(\frac{\partial \rho'}{\partial z'} \int_0^{2\pi} T' \, d\theta' + \frac{\partial T'}{\partial z'} \int_0^{2\pi} \rho' \, d\theta'\right) = -\mathscr{M}v_z' \int_0^{2\pi} \omega' \, d\theta' \tag{25}$$

Energy:

$$v_z' \frac{\partial T'}{\partial z'} \int_0^{2\pi} \rho' \, d\theta' + (\gamma - 1) \frac{\partial v_z'}{\partial z'} \int_0^{2\pi} P' \, d\theta' = \frac{8}{3} \pi\gamma(\gamma - 1) \mathscr{f} f(\gamma)\left(\frac{\partial v_z'}{\partial z'}\right)^2$$

$$+ \mathscr{M} \int_0^{2\pi} \omega'\left[(\gamma - T') + \gamma \frac{\gamma - 1}{2} v_z'^2\right] d\theta' - \mathscr{K} \int_0^{2\pi} (P' - 1) d\theta' \tag{26}$$

Ideal gas:

$$2\pi \frac{\partial P'}{\partial z'} = \frac{\partial \rho'}{\partial z'} \int_0^{2\pi} T' \, d\theta' + \frac{\partial T'}{\partial z'} \int_0^{2\pi} \rho' \, d\theta' \tag{27}$$

Introducing a pressure disturbance allows the evaluation of the axial derivatives with the use of equations (24) to (27). Then the pressure, temperature, particle velocity, density, and burning rate at various positions around the annulus can be calculated as functions of time by using equations (19) to (23). A burning rate expression, however, must be introduced before proceeding.

9

Burning Rate Expression

Uniform decomposition of the propellant is assumed around the circumference. Burning then occurs at some rate dependent on the position around the annulus and is accompanied by gas flow in the axial direction. The grain was assumed to decompose and to react in accordance with the normal strand rate expression with an additive erosive effect:

$$w = \frac{\rho_s}{2r_1}\left[CP^n + k(\rho v)^m\right] \qquad (28)$$

Quasi-steady behavior is assumed with no variation in the propellant response with frequency. Expression (28) is normalized by the average rate

$$w_0 = \frac{\rho_s}{2r_1}\left[CP_0^n + k(\rho_0 v_0)^m\right]$$

which yields

$$w' = (P')^n\left(\frac{1}{1+\epsilon}\right) + (\rho' v')^m\left(\frac{\epsilon}{1+\epsilon}\right) \qquad (29a)$$

where ϵ is the erosive contribution to the burning rate divided by the strand rate:

$$\epsilon = \frac{k(\rho_0 v_0)^m}{CP_0^n} \qquad (29b)$$

Now

$$(v')^m = \left(\frac{v}{v_0}\right)^m = \left(\frac{v_\theta^2 + v_z^2}{v_z^2}\right)^{m/2} = \left[1 + \left(\frac{v_\theta}{v_z}\right)^2\right]^{m/2} \qquad (30)$$

Substituting for $(v')^m$ into equation (29a) gives the instantaneous local burning rate, which is dependent on the amplitude of the pressure disturbance:

10

$$w' = \frac{1}{1 + \epsilon} (P')^n + \frac{\epsilon}{1 + \epsilon} (\rho')^m \left[1 + \left(\frac{v'_\theta}{v'_z} \right)^2 \right]^{m/2} \tag{31}$$

Technique for Numerical Solutions

The disturbance introduced consisted of an instantaneous adiabatic pressure change at time $t' = 0$ and is given by

$$\left. \begin{aligned} P' &= 1 + \frac{A_p}{2} \sin \theta' \\[2ex] T' &= \left(1 + \frac{A_p}{2} \sin \theta' \right)^{(\gamma - 1)/\gamma} \\[2ex] \rho' &= \left(1 + \frac{A_p}{2} \sin \theta' \right)^{1/\gamma} \\[2ex] v'_\theta &= 0 \end{aligned} \right\} \tag{32}$$

The disturbance introduced by equation (32) represents the first standing transverse (sloshing) mode in the annulus.

The input quantities that were specified for the numerical solution of the equations were the pressure disturbance amplitude A_p, the burning rate parameter $\mathcal{M}$, the axial Mach number of the gas flow v'_z, the amount of erosive burning ϵ, the pressure exponent n, the velocity exponent m, the ratio of specific heats γ, the wall loss factor $\mathcal{X}$, the viscous dissipation parameter $\mathcal{J}$. These specified quantities as well as the pressure, temperature, density, and tangential velocity expressions (eq. (32)) were substituted into the integrated forms of the conservation equations (24), (25), and (26); the ideal gas law (eq. (27)); and the burning rate expression (eq. (31)). Computer calculations of the axial derivatives were then made at 20 equally spaced positions around the annulus at a time t'. The numerical values of the axial derivatives were then substituted into the differential form of the conservation equations (19), (20), (21), (22), and the ideal gas relation (eq. (23)) to yield a solution for the pressure, temperature, and velocity at each annular position for a given time. The computational procedure was then repeated by using a time interval t' equal to 0.031. This time interval was such that meaningful results

could be obtained prior to the onset of computer noise. Computations were performed to a minimum of $t' = 4\pi$ and a maximum of $t' = 10\pi$, which represent twice and five times around the annulus, respectively. In order to determine whether the amplitude of the disturbance grew, remained constant, or decreased with time, the peak pressure minus the minimum pressure (at any chamber position) was plotted as a function of time. Growth of the disturbance was interpreted as an unstable condition; whereas an amplitude decay was indicative of a stable situation. Since the specified initial conditions yielded only a single point for a stability plot, it was necessary to make numerous calculations for a complete stability map. The line dividing the unstable region from the region of stability corresponded to the position of neutral stability. These results are discussed in the following section.

RESULTS AND DISCUSSION

Discussion of Solutions

The peak-to-peak amplitude of the pressure oscillations showed a very definite behavior dependent on the amplitude of the initial disturbance and the parameter $\mathscr{M}$. For those values of pressure amplitude and $\mathscr{M}$ that were very stable the oscillation quickly decayed to a low percentage of the chamber pressure within several cycles; whereas in the unstable regime the amplitude reached a value of 50 to 100 percent of the chamber pressure within a half cycle. In many cases the wave shape showed considerable distortion from sinusoidal behavior.

Combustion Sensitive to Pressure Only

Figure 2 shows the regions of stable and unstable operation obtained from observing the amplitude of the pressure disturbance with time. The ordinate represents the minimum disturbance required to cause the motor to become unstable for a given value of the burning rate parameter $\mathscr{M}$. At low values of the burning rate parameter $\mathscr{M}$ it was found that the system became unstable from small disturbances; whereas at higher $\mathscr{M}$ values an amplitude of approximately 10 percent was required to initiate instability. The erosive contribution in this case is zero, and hence the stability boundary is representative of a pure pressure response of the combustion. The axial Mach number v_z' is 0.01, which corresponds to some position near the head end of the combustion chamber. The pressure index n was 0.4, and the wall-loss parameter $\mathscr{X}$ was taken as 0.003. The viscous loss parameter $\mathscr{J}$ was set equal to 3×10^{-11} for all calculations.
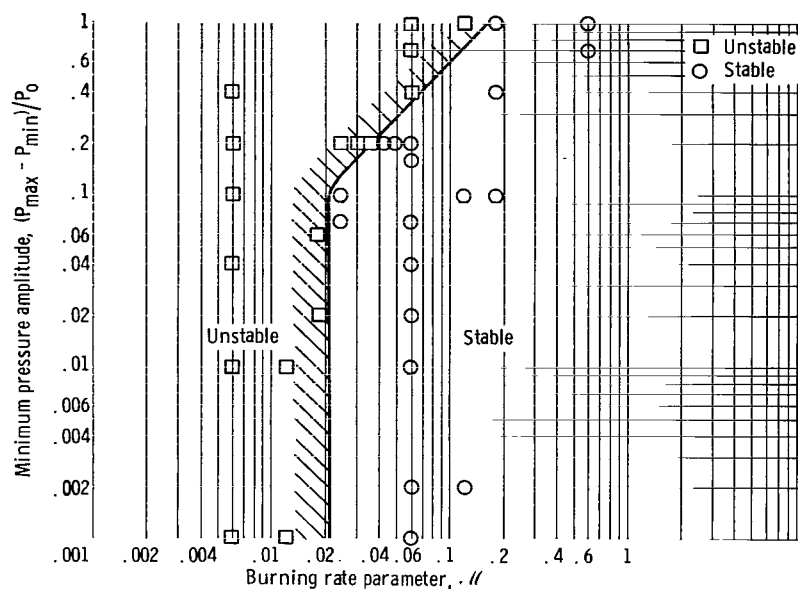
12

Figure 2. – Combustion stability limits for pressure response only. Pressure exponent, n = 0.4; erosive burning factor, $\epsilon = 0$; axial Mach number, $v'_z = 0.01$; viscous dissipation parameter, $\mathcal{Y} = 3 \times 10^{-11}$; wall-loss parameter, $\mathcal{K} = 0.003$.
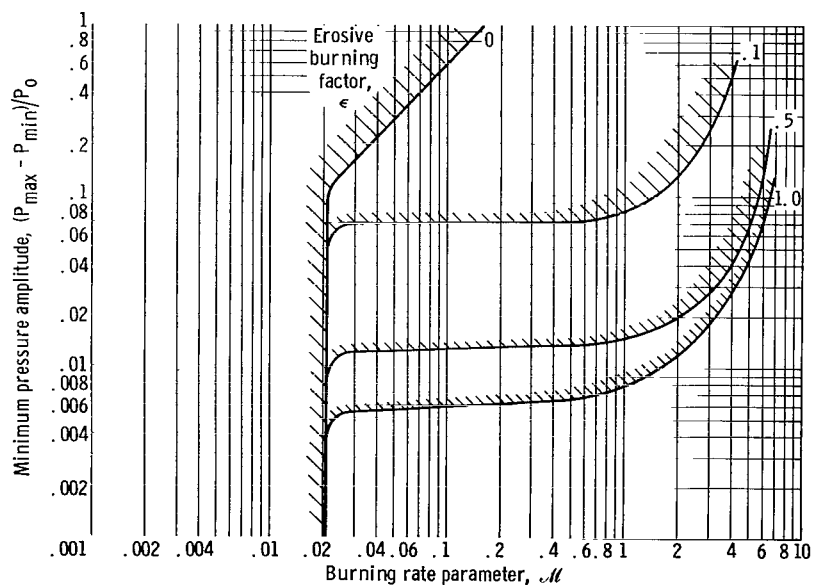

Figure 3. – Erosive burning effect on combustion stability limits. Pressure exponent, n = 0.4; velocity exponent, m = 0.8; axial Mach number, $v'_z = 0.01$. Unstable region is above and to the left of stability boundaries.

13

In order to arrive at a value of $\mathscr{X}$, the equation given in appendix B was evaluated for both a large scale motor (120-in. i. d. oscillating at 175 cps) and a small scale motor (4-in. i. d. oscillating at 5000 cps), both operating at a mean pressure of 750 pounds per square inch. The ratio of the inner to the outer diameter was taken as 0. 5, and the densities, speeds of sound, and viscosities for the gas and solid were those given in reference 16. The specific heat ratio was 1. 2. The value of the admittances thus calculated was in the neighborhood of 0.5×10^{-8} cubic foot per pound force second. In order to ascertain the effect of the wall-loss parameter, the stability map was calculated for values of $\mathscr{X}$ from zero to 0. 003, which is two orders of magnitude greater than that calculated from equation (B2) (appendix B). No change in the stability regime was found. Hence, in subsequent calculations the wall-loss parameter $\mathscr{X}$ was neglected. The analysis assumed no change in the wave characteristics due to interactions at the vibrating wall. The energy loss term was added in phase with the pressure.
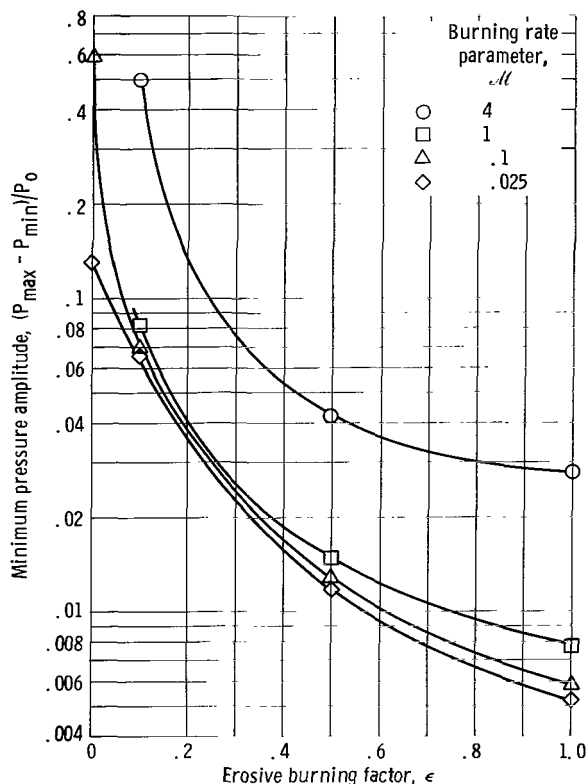

Figure 4. - Pressure disturbance required for instability as function of erosive burning factor. Pressure exponent, n = 0. 4; velocity exponent, m = 0. 8; axial Mach number, v'_z = 0. 01. Unstable region is above stability boundaries.

Combustion Sensitive to Pressure and Velocity

The effect of introducing erosive burning is illustrated in figure 3 where the erosive contribution to the burning rate divided by the strand rate ϵ is 10, 50, and 100 percent and the velocity exponent m is 0. 8. For ϵ = 0. 1, the stability boundary above a pressure amplitude of 7 percent is changed drastically from that of pure pressure response of the burning rate (fig. 2). Increasing ϵ to 0. 5 and 1 reduces the zone of stable motor operation considerably and thereby enchances the occurrence of instability. Erosion appears, therefore, to have an extremely important influence on the stability behavior of a rocket system. Figure 4 shows the stability results as a function of the erosive factor. As a comparative measure of the pressure and velocity effects, the burning rate exponent n
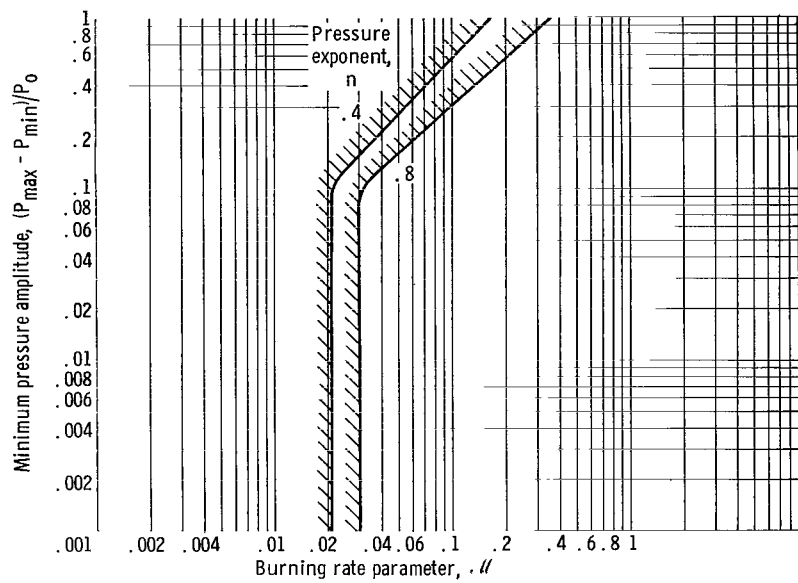
Figure 5. – Effect of pressure exponent on combustion stability limits. Axial Mach number, $v_z' = 0.01$; erosive burning factor, $\epsilon = 0$. Unstable region is above and to the left of stability boundaries.
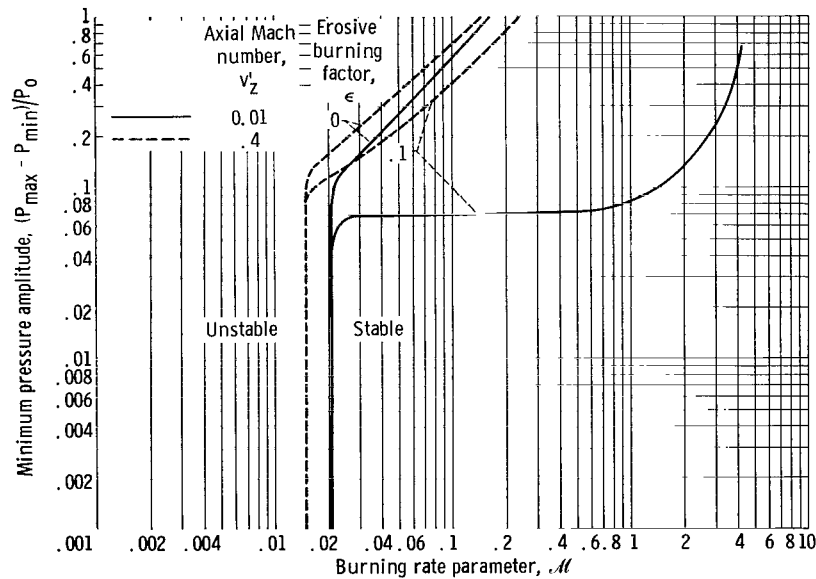

Figure 6. – Axial velocity effect on combustion stability limits. Pressure exponent, n = 0.4; velocity exponent, m = 0.8. Unstable region is above and to the left of stability boundaries.

was assigned a value of 0.8, equivalent to the erosive velocity exponent. Figure 5 shows that the resulting stability boundary has been shifted downward and toward the right, which reduces the region of stable operation. Hence the higher burning rate propellant would have a greater tendency toward unstable behavior than would the low burning rate propellants. The change in the stability boundary caused by the pressure exponent is not nearly as large as that caused by erosive burning of only 10 percent. Thus, erosive burning with pressure sensitivity appears to represent a more critical parameter for determining motor stability than pure pressure responsiveness.

Port Mach Number Effect

The effect of axial Mach number on stability, as shown in figure 6, revealed increased stability with increasing flow velocity through the motor cavity. At a Mach number v_z' of 0.4, the stable region was slightly increased compared with that at a Mach number of 0.01. The stabilizing effect of the axial velocity was seen most effectively for the case where the erosive contribution ϵ was equal to 0.1. With a Mach number v_z' of 0.01, a change in ϵ from 0 to 0.1 drastically reduced the stability boundary; whereas with a Mach number of 0.4 the effect of changing ϵ from 0 to 0.1 was to reduce the stability limits only a slight amount. For very low values of the axial velocity (e.g., 0.0001) the entire map was found to be unstable at every $\mathscr{M}$ and $\Delta p/p$ value for both $\epsilon = 0$ (pressure response only) and $\epsilon = 0.1$ (pressure and erosive velocity responses). The stabilizing influence of axial flow velocity was probably due to the fact that the vectorial addition of the axial Mach number v_z' and the tangential Mach number v_θ' is virtually independent of the magnitude of v_θ' unless v_z' becomes very small. At low values of v_z', the mean flow through the combustor was then significantly affected by v_θ'. It is likely that the axial Mach number was higher than 0.0001 because of the existence of recirculating flow or the presence of turbulence near the head cavity.

Chemical Kinetic Calculation

If propellant burning is assumed to follow an Arrhenius relation rather than expression (31), the equations to be solved reduce exactly to those used in reference 14. Then the results of reference 14 can be compared with those obtained herein. Figure 7 shows the results of reference 14, which used the Arrhenius rate law (chemical kinetic model), and the results obtained in this study with expression (31). The figure shows that for the chemical kinetic model to be dominant in predicting the stability boundary it is necessary to have an unreacted gas-phase concentration of approximately 10 percent.
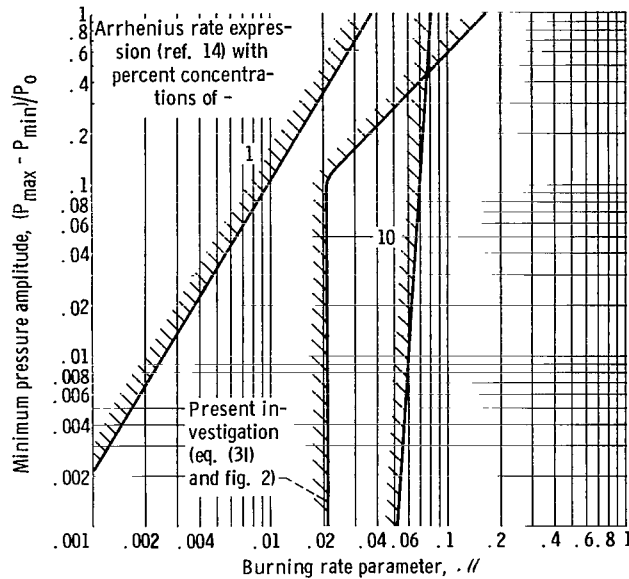
16

Figure 7. - Comparison of stability limits by using Arrhenius rate expression (ref. 14) and equation (31) of present investigation. Unstable region is above and to the left of stability boundaries.

System Losses and Stability

Changes in the viscous-dissipation parameter $\mathcal{J}$ are not expected to change the stability limits since the shear stresses $\mu(\partial v_\theta/\partial_\theta)$ in the one-dimensional model are negligible; hence the damping produced by viscous forces would not be significant. In reference 14, $\mathcal{J}$ was varied by four orders of magnitude with no resulting effect on stability. A variation in γ from 1.0 to 1.5 also did not affect the results. Losses due to the presence of the head- and nozzle-end cavities were not considered, but they might be effective in shifting the stability boundaries to lower values of $\mathcal{M}$, thus increasing the stable operating region.

The stability of a three-dimensional combustor cannot be determined by this analysis. Beltran and Frankel (ref. 17) have used the analysis, however, to find the most sensitive region in a combustor by varying the radius and axial velocity. In reference 17 the most sensitive region was assumed to determine overall engine stability. Recent studies by Priem and Reese (unpublished NASA data) have shown that with a two-dimensional geometry consisting of a long annulus the overall stability is generally determined by the most sensitive zone. It is anticipated, therefore, that overall motor stability can be determined by locating the most sensitive region in the combustor. The two-dimensional stability boundaries are somewhat restricted relative to the one-dimensional results (Priem and Reese, unpublished NASA data).

17

CONCLUDING REMARKS

Based on the foregoing results, both the amplitude of the pressure disturbance and the $\mathcal{M}$ value, as well as the amount of erosive burning, must be known to predict relative combustion stability in solid rocket motors. A further requirement is that the changes in these parameters with motor running time must be known. As a solid rocket grain burns and its dimensions change, the location on the stability plot may shift to the right or left or remain at a constant value of $\mathcal{M}$. At the same time the axial flow velocity is being influenced by the change in the cavity dimension. For an internally burning cavity with increasing port diameter the axial Mach number and the amount of erosive burning will decrease with time. The pertinent stability boundary must be used as indicated by the value of ϵ. If a variation in the amplitude of the disturbance occurs during motor operation, a change in the location of the motor operating point on the stability map will result. It is evident, therefore, that as the dimensions of a motor grain change with operating time various attendant changes occur so that the operating condition of the motor is located in stable or unstable regimes. This yields an explanation for the appearance and disappearance of instability during a rocket motor firing.

Finally, it was demonstrated that the gas phase attenuation and nozzle losses would damp out a pressure disturbance in the absence of a driving force, namely a zero pressure exponent on the burning rate and a zero erosive contribution.

SUMMARY OF RESULTS

A one-dimensional, nonlinear analysis of transverse mode instability in a solid propellant rocket geometry indicated the relative combustion stability based on three parametric groupings: burning rate, wall-loss, and viscous-dissipation parameters, of which only the burning rate parameter appeared to be significant in the one-dimensional model with a nonvibrating solid phase. The results of the analysis, presented as the minimum pressure amplitude required to incite instability as a function of the burning rate parameter, showed that erosive burning was an important factor in determining stability. With only a 10-percent contribution to the burning rate due to erosion, the stability boundary was significantly affected so as to reduce the stable region of operation. A two-fold increase in the pressure exponent in the burning rate law also showed a decrease in the stable operating regime. This effect was not as pronounced as the erosive effect. Increasing the axial flow velocity was found to enhance stability. At a Mach number of 0.0001, with either zero- or 10-percent erosion, no stable operating condition was

found. The results of the analysis yielded an explanation for the appearance and disappearance of instability during a rocket motor firing.

Lewis Research Center,
    National Aeronautics and Space Administration,
        Cleveland, Ohio, February 4, 1966.

APPENDIX A

SYMBOLS

A_p peak-to-peak pressure disturbance, $(P_{max} - P_{min})/P_o$

A_s propellant burning area, ft^2

A_t nozzle throat area, ft^2

a average speed of sound in gases, ft/sec

a_s speed of shear waves in solid, ft/sec

a_d speed of dilational waves in solid, ft/sec

C strand burning rate constant

c_p specific heat at constant pressure, Btu/(lb)(^{o}F)

c_v specific heat at constant volume, Btu/(lb)(^{o}F)

c^* characteristic exhaust velocity, ft/sec

E_d viscoelastic wall losses (defined in eq. (4))

f frequency of oscillation, radians/sec

$f(\gamma)$ function of gamma, $\sqrt{\left(\dfrac{2}{\gamma + 1}\right)^{\gamma+1/\gamma-1}}$

g acceleration due to gravity, 32.2 ft/sec^2

J mechanical equivalent of heat

$J_m()$ Bessel function

$\mathcal{J}$ viscous dissipation parameter, $\mu_o c^*/RP_o g$

k erosive burning rate constant

k_c wave number for compression wave in solid, f/a_d

k_g wave number for sound wave in gas, f/a

k_s wave number for equivoluminal wave in solid, f/c_s

K propellant surface area throat area, A_s/A_t

$\mathcal{K}$ wall-loss parameter, $P_o^2 r Z_1/\rho_o c_v T_o a$

M molecular weight of gas, lb mass/lb mole

$\mathcal{M}$ burning rate or K ratio parameter, $2\rho_s r_s/\rho_o a$ or $(2/K)f(\gamma)$

$\bar{m}$ mode number in solid phase

P pressure, lb/ft^2

R universal gas constant, 1544 (ft)(lb force)/(^{o}R)(mole)

r annular radius, ft

r_s regression rate of propellant, ft/sec

S_r displacement vector

T gas temperature, ^{o}R

t time, sec

U_s	internal energy of solid, Btu/lb
V	combustor volume, ft^3
v	gas velocity, ft/sec
w	propellant mass addition rate, lb/sec
Z_1	acoustic admittance factor (see eq. (9))
γ	specific heat ratio, c_p/c_v
ϵ	erosive burning factor (eq. (29b))
η	shear viscosity of solid, 0.4 (lb)(sec)/ft^2
λ	thermal conductivity of gases, Btu/(ft)(sec)($^\circ$F)
λ_1	dilational viscosity of solid, 0.4(lb)(sec)/ft^2
μ	gas viscosity, lb/(ft)(sec)
ρ	gas density, lb/ft^3
ρ_s	solid density, lb/ft^3
τ	stress tensor, lb/(ft)(sec^2)
ω	local instantaneous burning rate, lb/(sec)(ft^3)
∇	differential operator, $(ft)^{-1}$

Subscripts:

max	maximum
min	minimum
o	steady state
r	radial coordinate
z	axial coordinate
θ	angular coordinate
1	inside diameter of propellant grain
2	outside diameter of propellant grain

Superscripts:

m	velocity exponent (see eq. (28))
n	pressure exponent (see eq. (28))
'	reduced parameter, instantaneous value divided by the steady-state value (see eq. (6))
$\rightarrow$	vector

APPENDIX B

DISSIPATION OF WAVE ENERGY IN SOLID PROPELLANT

The amount of energy that would be lost if the solid were vibrating can be determined. The maximum energy loss would occur if the pressure and outward wall velocity were exactly in phase. The model used is one dimensional in θ, and hence mass and momentum losses in the radial direction were not completely included in the conservation equations. Since energy is not a directed quantity, a loss term may be added to the energy equation. A linear analysis of acoustic gains and losses, including all terms in the conservation equations, has been carried out. The dissipation of elastic wave energy in the cylindrical grain may be determined from the results of Bird (ref. 15) and Bird, Hart, and McClure (ref. 16):

The dissipation rate per unit length of solid wall is

$$E_d = \frac{\pi r_1}{2} J_m^2(k_g r_1) \left| \frac{A_p}{2} \right|^2 \text{real part}\left(\frac{ifS_r}{-P_{rr}} \right)_{r_1} \tag{B1}$$

where r_1 is the inside radius of the propellant grain, S_r is a displacement vector and P_{rr} is a stress tensor in the solid grain. Substituting the approximations given in reference 15 for the real part of the specific acoustic admittance into equation (B1) gives:

$$E_d = \frac{\pi r_1 J_m^2(k_g r_1) \left| \frac{A_p}{2} \right|^2 f^2 (r_2 - r_1)}{4 \rho_s^2 a_d^4 \cos^2 \frac{f}{a_d}(r_2 - r_1) \cos^2 \frac{f}{a_s}(r_2 - r_1)} \left(\left[1 + \frac{\sin \frac{f}{a_d}(r_2 - r_1) \cos \frac{f}{a_d}(r_2 - r_1)}{\frac{f}{a_d}(r_2 - r_1)} \right] \right.$$

$$\times \left[\cos \frac{f}{a_s}(r_2 - r_1) + \left(\frac{4\overline{m}^2 + 15}{8\alpha_s} - \frac{4\overline{m}^2 + 3}{8\beta_s} \right) \sin \frac{f}{a_s}(r_2 - r_1) \right]^2 \left(\lambda_1 + \frac{4}{3} \eta \right)$$

$$+ \left\{ \overline{m}^2 \eta \frac{a_d^3}{a_s^3} \left[\frac{1}{k_s k_c r_2^2} - \frac{4 \sin \frac{f}{a_d}(r_2 - r_1) \sin \frac{f}{a_s}(r_2 - r_1)}{k_s^2 r_1 r_2} \right] \right.$$

$$\left. + 4 \frac{a_s}{a_d} \frac{\sin^2 \frac{f}{a_d}(r_2 - r_1)}{k_s^2 r_1^2} + \frac{4}{\overline{m}^2} \frac{a_s}{a_d} \frac{\sin^2 \frac{f}{a_d}(r_2 - r_1) \cos^2 \frac{f}{a_s}(r_2 - r_1)}{\frac{f}{a_s}(r_2 - r_1) k_s r_1} \right\} \right) \tag{B2}$$

where r_2 is the outside radius of the propellant grain, and r_1 is the inside radius. This wall-loss term gives a dissipation rate per unit length of propellant around the inside perimeter and must be multiplied by a factor of $2/r_1$ in order to obtain a rate of energy loss per unit volume of gas. The term is then subtracted from the right side of the energy equation (3).

REFERENCES

1. Trubridge, G. F. P.: Unstable Burning in Solid Propellant Rocket Motors. J. Brit. Interplanet. Soc., vol. 20, No. 2, Mar.-Apr. 1965, pp. 33-42.

2. Hart, R. W.; and McClure, F. T.: Theory of Acoustic Instability in Solid-Propellant Rocket Combustion. Tenth Symposium (International) on Combustion. Combustion Institute, 1965, pp. 1047-1065.

3. Price, E. W.: Experimental Solid Rocket Combustion Instability. Tenth Symposium (International) on Combustion. Combustion Institute, 1965, pp. 1067-1080.

4. Berl, W. G.; Hart, R. W.; and McClure, F. T.: Solid Propellant Instability of Combustion. Rep. no. TG371-8A, Johns Hopkins University, July 1964.

5. Price, E. W.: Review of the Combustion Instability Characteristics of Solid Propellants. Preprint of the 25th Meeting AGARD Combustion and Propulsion Panel, San Diego, California, Apr. 1965.

6. McClure, F. T.; Hart, R. W.; and Bird, J. F.: Acoustic Resonance in Solid Propellant Rockets. J. Appl. Phys., vol. 31, no. 5, May 1960, pp. 884-896.

7. Horton, M. D.; and Price, E. W.: Dynamic Characteristics of Solid Propellant Combustion. Ninth Symposium (International) on Combustion, Academic Press, New York, 1963, pp. 303-310.

8. Strittmater, R.; Watermeier, L.; and Pfaff, S.: Virtual Specific Acoustic Measurements of Burning Solid Propellant Surfaces by a Resonant Tube Technique. Ninth Symposium (International) on Combustion, Academic Press, 1963, pp. 311-315.

9. Cantrell, R. H.; McClure, F. T.; and Hart, R. W.: Effects of Thermal Radiation on the Acoustic Response of Solid Propellants. AIAA J., vol. 3, no. 3, March 1965, pp. 418-426.

10. Hart, R. W.; Bird, J. F.; Cantrell, R. H.; and McClure, F. T.: Nonlinear Effects in Instability of Solid-Propellant Rocket Motors. AIAA J., vol. 2, no. 7, July 1964, pp. 1270-1273.

11. McClure, F. T.; Hart, R. W.; and Bird, J. F.: Solid Propellant Rocket Motors as Acoustic Oscillators. Vol. I of Progress in Astronautics and Rocketry, M. Summerfield, ed., Academic Press, 1960, pp. 295-358.

12. Bird, J. F.; McClure, F. T.; and Hart, R. W.: Acoustic Instability in the Transverse Modes of Solid Propellant Rockets. 12th International Astronautical Congress, Robert M. L. Baker, Jr., and Maud W. Makemson, eds., Academic Press, Inc., 1963, pp. 459-473.

13. Hart, R. W.; and Bird, J. F.: Scaling Problems Associated with Unstable Burning in Solid Propellant Rockets. Ninth Symposium (International) on Combustion, Academic Press, 1963, pp. 993-1004.

14. Priem, Richard J.; and Guentert, Donald C.: Combustion Instability Limits Determined by a Nonlinear Theory and One-Dimensional Model. NASA TN D-1409, 1962.

15. Bird, J. F.: Vibrations of Thick-Walled Hollow Cylinders: Approximate Theory. J. Acoust. Soc. Am., vol. 32, no. 11, Nov. 1960, pp. 1413-1419.

16. Bird, J. F.; Hart, R. W.; and McClure, F. T.: Vibrations of Thick-Walled Hollow Cylinders: Exact Numerical Solutions. J. Acoust. Soc. Am., vol. 32, no. 11, Nov. 1960, pp. 1404-1412.

17. Beltran, M. R.; and Frankel, N. A.: Prediction of Instability Zones in Liquid Rocket Engines. AIAA J., vol. 3, no. 3, March 1965, pp. 516-518.

NASA SCIENTIFIC AND TECHNICAL PUBLICATIONS

TECHNICAL REPORTS: Scientific and technical information considered important, complete, and a lasting contribution to existing knowledge.

TECHNICAL NOTES: Information less broad in scope but nevertheless of importance as a contribution to existing knowledge.

TECHNICAL MEMORANDUMS: Information receiving limited distribution because of preliminary data, security classification, or other reasons.

CONTRACTOR REPORTS: Technical information generated in connection with a NASA contract or grant and released under NASA auspices.

TECHNICAL TRANSLATIONS: Information published in a foreign language considered to merit NASA distribution in English.

TECHNICAL REPRINTS: Information derived from NASA activities and initially published in the form of journal articles.

SPECIAL PUBLICATIONS: Information derived from or of value to NASA activities but not necessarily reporting the results of individual NASA-programmed scientific efforts. Publications include conference proceedings, monographs, data compilations, handbooks, sourcebooks, and special bibliographies.

Details on the availability of these publications may be obtained from:

SCIENTIFIC AND TECHNICAL INFORMATION DIVISION

NATIONAL AERONAUTICS AND SPACE ADMINISTRATION

Washington, D.C. 20546